Aerated Vibrofluidization of Silica Nanoparticles

Caroline H. Nam and Robert Pfeffer
Dept. of Chemical Engineering, New Jersey Institute of Technology, Newark, NJ 07102

Rajesh N. Dave
Dept. of Mechanical Engineering, New Jersey Institute of Technology, Newark, NJ 07102

Sankaran Sundaresan
Dept. of Chemical Engineering, Princeton University, Princeton, NJ 08544

DOI 10.1002/aic.10237
Published online in Wiley InterScience (www.interscience.wiley.com).

Vigorous homogeneous fluidization of 12-nm silica particles was easily achieved by coupling aeration with vibration. Vibration (with frequency in the range of 30 to 200 Hz, and vibrational acceleration in the range of 0 to 5 g) was found to be necessary to achieve smooth fluidization. The minimum fluidization velocity, defined as the lowest gas velocity at which the pressure drop across the bed reaches a plateau, was approximately 0.3–0.4 cm/s, and essentially independent of the vibrational acceleration. However, the bed expanded almost immediately after the air was turned on, reaching bed expansions of three times the initial bed height or higher. Thus the bed appeared to exhibit a fluidlike behavior at velocities much lower than the minimum fluidization velocity. Fluidization of nanoparticles was achieved as a result of the formation of stable, relatively large, and very porous agglomerates. Practically no bubbles or elutriation of particles was observed. A fractal analysis combined with a modified Richardson–Zaki approach is proposed for prediction of agglomerate size and voidage. © 2004 American Institute of Chemical Engineers
AIChE J, 50: 1776–1785, 2004
Keywords: nanoparticles, fluidization, vibration, fractal structure, agglomerates, high porosity

Introduction

During the past decade, nanoparticles and nanocomposites have become the focus of many research papers because of the unique properties of nanostructured materials that make them attractive to various industrial applications. When a material is made from nanoparticle building blocks, catalytic, mechanical, electronic, optical, and other physical and chemical properties are significantly, and often favorably, altered. To create advanced nanostructured materials with unique tailored properties, it is often necessary to form nanocomposities, which include homogeneous mixtures of nanoparticles, or nanometer particles coated with or dispersed in a matrix of another material such as a polymer. For example, it might be desirable to coat an ultrathin film of a biodegradable polymer onto the surface of nanosized drug particles to make them time release. Before coating can take place, however, the nanosized particles have to be well dispersed. Fluidization is one of the best techniques available to disperse and process powders, but nanoparticles are very difficult to fluidize because of their small size and cohesive properties.

Gas fluidization of powders has usually been restricted to Geldart (1973) group A and B powders. Finer particles in the group C range ($<30\ \mu$m) are difficult to fluidize because of the strong interparticle (cohesive) forces between them. A number of studies (Chaouki et al., 1985; Iwadate and Horio, 1998;

Correspondence concerning this article should be addressed to R. Pfeffer at robert.pfeffer@njit.edu.

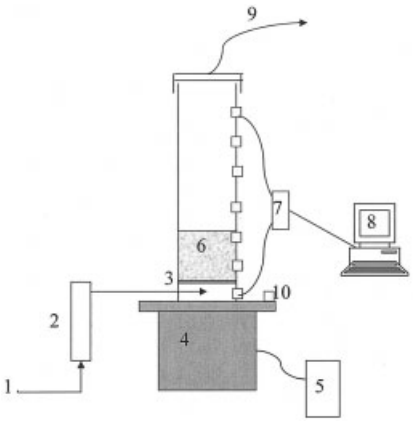

Figure 1. Experimental apparatus.

1: Compressed air; 2: rotameter; 3: distributor; 4: vibrator; 5: inverter; 6: fluidized bed; 7: pressure transducer; 8: computer; 9: vent; 10: accelerometer.

Morooka et al., 1988; Pacek and Nienow, 1990; Wang, Y., et al., 2002; Wang, Z., et al., 1998; Zhou and Li, 1999) have been conducted to investigate the fluidization of ultrafine particles in conventional fluidized beds. Some of these investigators used nanoparticles, which are at the extreme end of Geldart group C powders. It has been observed that group C particles including nanoparticles can sometimes be fluidized in the form of agglomerates, and has been called "agglomerating fluidization" by Iwadate and Horio (1998). However, the formation of agglomerates and agglomerating fluidization occur at a superficial velocity well above the theoretical minimum fluidization velocity. The work reported in the literature thus far includes experiments and theoretical modeling of hydrodynamic behavior and agglomerate size.

It has been shown that adding mechanical agitation such as acoustic waves (Chirone et al., 1993; Herrera et al., 2002) or vibration (Dutta and Dullea, 1991; Jaraiz et al., 1992; Malhotra and Mujumdar, 1987; Marring et al., 1994, 1995; Mawatari et al., 2002; Mori et al., 1990; Noda et al., 1998; Tasirin and Anuar, 2001; Valverde et al., 2001a; Venkatesh et al., 1998; Wank et al., 2001; Youzhi et al., 1998) can improve the fluidization of micron size Geldart group C cohesive powders. It has been observed that the addition of vibration helps to eliminate the characteristic cracking, channeling, and rising as a plug, when group C powders are aerated in a conventional fluidized bed. Previous fluidization studies have used powders whose sizes ranged from submicron to a few millimeters. To our knowledge the use of nanoparticles in the present study, subject to vibration and aeration, has not been previously reported. In this communication, phenomenological observations of the vibrofluidization of silica nanoparticles silica are presented. The experimental results are compared with a simple model to capture the size and other important properties of the agglomerates that were formed during the fluidization process.

Experimental

The experimental apparatus is illustrated in Figure 1. The fluidized bed consisted of a glass tube with an inner diameter of 6.25 cm and height of 35 cm, equipped with a series of ports for sampling and pressure measurements. The distributer consisted of a porous glass material. A sintered metal disc was originally used but the measured pressure drop across it was too high relative to the pressure drop across the nanoagglomerates. The bed was mounted on top of a Ling Dynamic System vibrator, which can produce AC vertical sinusoidal waves with accelerations up to $5.5g$ (where g is the acceleration attributed to gravity) measured by a piezoelectric accelerometer. The frequency (f) of vibration could be varied from 30 to 200 Hz. The powder used was Aerosil R974 (Degussa) hydrophobic silica, whose primary particle size, particle density, bulk density, and external surface area were 12 nm, 2200 kg/m^3, 30 kg/m^3, and 200 m^2/g, respectively. These silica nanoparticles are clearly at the extreme end of Geldart's group C powder classification. Comparative studies of different nanoparticles will be discussed in a separate report.

Humidity is an important issue when dealing with powders (especially hydrophilic powders) because of liquid bridges and electrostatic effects. However, in the experiments described below, we used hydrophobic silica, where humidity does not play as large a role, and bone-dry compressed air as the fluidizing gas. The airflow rate was measured by a rotameter. When the bed was in its typical mode of aeration (that is, channeling, lifting as a plug), the vibration was turned on. Flow rate, pressure drop, vibrational acceleration, frequency and bed height measurements, as well as visual observation of the fluidization behavior for each experiment were all recorded. The vibration *intensity* is defined as the ratio of vibrational acceleration to gravitational acceleration, $\Gamma = (A\omega^2)/g$, where A is the amplitude of vibration and $\omega = 2\pi f$. The pressure drop was measured by a pressure transducer and recorded on a computer. Photos were taken with a digital camera.

Two methods of sampling were used, both of which yielded similar results when the powder samples were viewed by a scanning electron microscope (SEM). The first involved aspirating out samples at different heights of the bed through small openings along the side of the tube. These samples were then gently placed on SEM sample disks. The second method consisted of gently dipping a SEM sample disk adhered with a double-sided carbon tape into the fluidized bed. The sample disk was then directly used for SEM analysis. In addition, to aid in viewing agglomerates in situ, an argon laser generator (Reliant 1000M, LaserPhysics) with 3-W power, and equipped with a high-speed CCD camera with an extremely short exposure time, was used.

Results and Discussion

It was observed experimentally that mechanical vibration helped break up the channeling and spouting in a bed of nanosized powders. Figure 2 illustrates a typical experiment.

Previous studies on micron-sized powder fluidization (Iwadate and Horio, 1998; Pacek and Nienow, 1990; Zhou and Li, 1999) and previous studies on nanoparticle fluidization (Chaouki et al., 1985; Morooka et al., 1988; Wang, Y., et al., 2002; Wang, Z., et al., 1998) have shown that formation of agglomerates and their fluidization could be achieved at gas velocities well in excess of the minimum fluidization velocity, based on the diameter of the nanoparticles. Considerably smaller gas velocities (but still much larger than that based on the primary nanoparticle size) were adequate in our experiments, given that

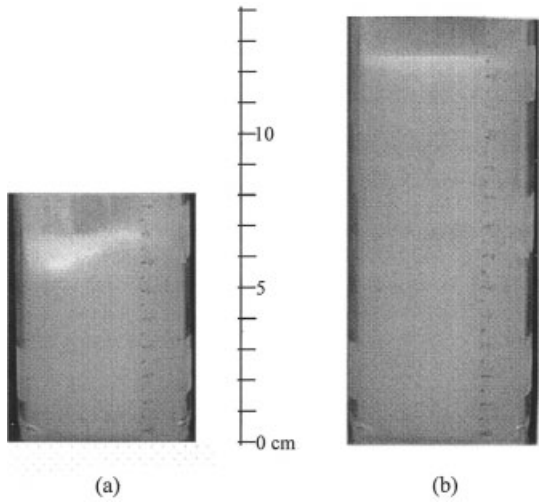

Figure 2. Typical photographs of aerated beds.

(a) Without vibration; (b) with vibration.

vibration provided sufficient energy to the system to overcome interparticle forces and form stable agglomerates.

Visual observation of a highly expanded bed revealed the presence of two distinct layers: a small bottom layer, consisting of very large agglomerates; and a larger top layer, consisting of very smoothly fluidized smaller agglomerates. SEM micrographs indicated that the fluidized agglomerates in the top layer ranged in size from approximately 5 to 50 μm. The bottom layer consisted of agglomerates that were measured to be as large as 2 mm. When the two layers were separated by aspirating out the smoothly fluidized agglomerates, and this top portion was reused as the next bed, the bottom dense layer did not reappear. This suggests that the dense layer simply contained the *hard* agglomerates, which were present in the as-received nanoparticles; such hard agglomerates could have formed during handling and storage. Under vibration, these large agglomerates would sink to the bottom of the bed because the vibration energy was not sufficient to break them up and the airflow was not large enough to fluidize them. To avoid a large agglomerate size distribution, only the top portion of the bed (smooth layer) was used in all of our experiments described below. It will be shown in a future paper that the dense phase can be eliminated without physical separation of the layers through the use of an external magnetic force coupled with gas flow to fluidize the nanoparticles.

A Beckman Coulter counter (dry module) was used to determine the agglomerate size distribution of the as-received silica powder. Representative Coulter counter results for pre-experiment powder indicated a mean agglomerate size of about 30–40 μm. This is highly suspect because large agglomerates of size on the order of millimeters (perhaps formed during storage) could be observed visually. These contradictory results suggest that the agglomerates are in general so fragile that any measurement method involving direct contact with the sample is not effective and reliable. We believe that the agglomerates were broken up during the course of our Coulter counter size distribution measurements, leading to agglomerate sizes of about 30–40 μm.

As mentioned above, agglomerate samples were aspirated out of the bed at different heights of the expanded fluidized bed and examined under SEM. As shown in Figure 3, the agglomerate sizes averaged about 30 μm. However, the agglomerates appeared very porous and fragile, and might have broken during their removal from the bed and/or during sample preparation for the SEM. As discussed later, the agglomerate size estimated from pressure drop and bed height data in fluidization experiments was considerably larger ($\sim$160 μm).

Given the fragile nature of the agglomerates, it is reasonable to expect that an equilibrium between agglomerate breakage and agglomerate formation is reached during the process of fluidization. Therefore, the true agglomerate size can be found only from measuring the agglomerates dynamically as fluidization is occurring. The use of a high-speed digital camera with an extremely short exposure time and a laser beam is currently being investigated to estimate the dynamic agglomerate size in situ.

A preliminary result of the camera and laser is shown in Figure 4. The laser beam was located at the surface of the vibrofluidized bed and the camera focused at the beam. The camera was positioned near the opening of the tube where a mirror was angled at 45°. In this way, no sources of possible distortion, such as the bed wall, would affect the image. Bright spots indicate agglomerates directly in line with the laser beam and therefore are focused. Grayer spots indicate agglomerates that are not quite in focus. The bright agglomerates in Figure 4

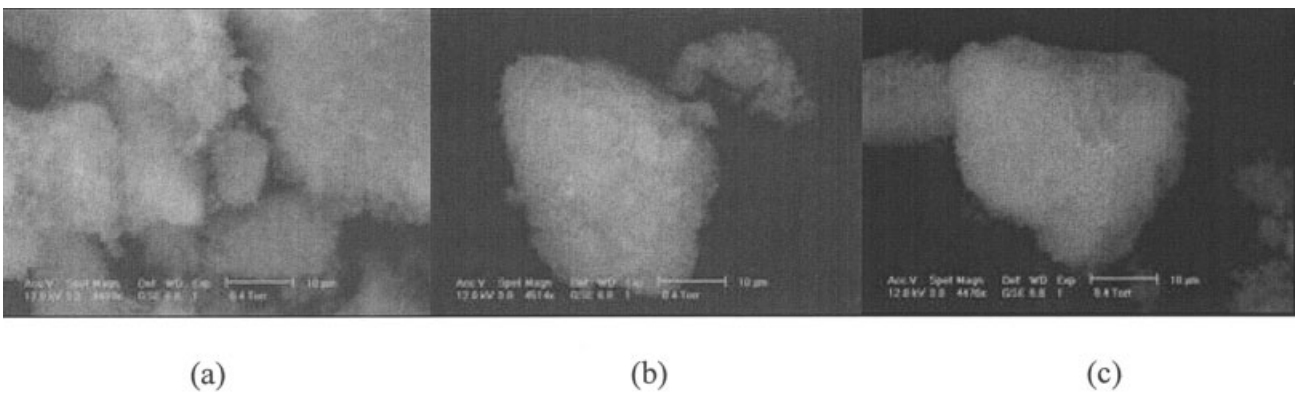

Figure 3. SEM images of samples taken during fluidization.

(a) Near the surface of the bed; (b) middle of the bed; and (c) toward the bottom of the bed.

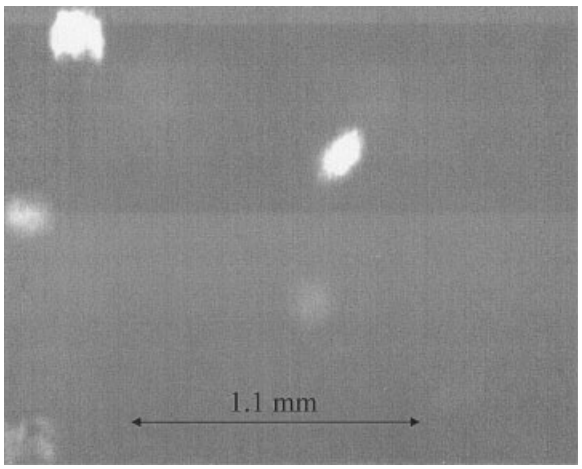

Figure 4. Preliminary laser and camera result capturing agglomerates (bright spots) in a vibrofluidized bed.

$\Gamma = 3, f = 50$ Hz.

measure approximately 150–220 microns, thus supporting our method of size estimation discussed in a later section.

Another interesting result was that, although this bed was not initially (before application of vibration) fluidizable with aeration alone, the bed appeared to have a short-term memory after vibration was applied. This memory effect was apparent in an experiment where the bed was first fully fluidized with vibration and aeration, and then was allowed to settle down by turning off the vibration and aeration. This settled bed could then be fluidized by aeration alone as long as it was done within a few minutes, which is not what one would expect given the Geldart group C character of the primary particles. Thus, once the bed was fluidized, the interparticle networks in the original sample were disrupted and the resulting agglomerates did not form strong cohesive networks for several minutes, even after the bed was allowed to settle. However, if the bed was left longer than a few minutes in its rest state, it became difficult to fluidize the bed.

Additionally, once the bed was fluidized with the aid of vibration and aeration, the vibration could be turned off and the bed would remain expanded and fluidized for a considerable amount of time ($\sim$30 h). Figure 5 shows a comparison between the settling of a fully expanded bed after (1) aeration was left on and vibration was turned off and (2) both aeration and vibration were turned off. Without both vibration and aeration, the bed collapsed to its initial height within 2 min. Based on the above experimental observations, it is conjectured that once the interparticle forces are disrupted, it takes a finite time to return to the original undisturbed conditions.

Fluidization behavior

According to Geldart et al. (1973), the type of fluidization behavior exhibited by particles depends on their size and the density difference between the particles and the fluidizing gas. Based on empirical observations, Geldart et al. (1973) determined that particles whose diameter is smaller than 30 μm and density difference is smaller than 1000 kg/m^3, classified as group C powders, are difficult to fluidize in a conventional gravity-driven fluidized bed. Generally, these powders would form cracks, channels, or lift as a solid plug when exposed to a fluidizing gas at low superficial gas velocity. This behavior is mainly caused by the strong interparticle (van der Waals) forces. The importance of these interparticle forces relative to the weight of the particle increases as the surface-to-volume ratio increases and may significantly exceed the external mechanical forces (such as that attributed to gravity) to which the particles are subjected. As stated previously, a few research groups (Chaouki et al., 1985; Iwadate and Horio, 1998; Li et al., 1990; Morooka et al., 1988; Pacek and Nienow, 1990; Wang, Y., et al., 2002; Wang, Z., et al., 1998; Zhou and Li, 1999) found that once a high enough superficial gas velocity was reached, the interparticle networks were disrupted and agglomerates or loosely bound structures of the ultrafine particles formed. It has been observed that those agglomerates could be fluidized with or without bubbles. Some studies (Iwadate and Horio, 1998; Wang et al., 1998; Zhou and Li, 1999) were conducted to examine this phenomenon as well as to estimate agglomerate sizes for cohesive powders during fluidization.

In this study, the bed of nanoparticles, when aerated without vibration, exhibited the aforementioned behavior of plug flow, channeling, and spouting. When airflow was coupled with sufficient vibration [so that $\Gamma = (A\omega^2)/g > 1$], the immobile bed would almost immediately begin to expand; the channels would close, the spouting would stop, and/or the solid plug would break up. Increasing vibrational intensity Γ weakly affected bed height. Figure 6 shows an instance of relatively large bubbles in a bed of nanoparticles where the bottom dense and top smooth phases had not yet been separated. The same phenomenon was also seen when only the top portion of the bed was used. At high vibration frequencies ($f > 100$ Hz) and airflow rate, relatively large bubbles could be seen (see Figure 6). At low frequencies ($<$50 Hz), many of the bubbles appeared to break and dissipate throughout the bed, forming microbubbles (estimated to be about 200 μm). Bubbles were not seen to coalesce, grow, or break the upper surface of the bed.

At modest fluidization gas velocities, the surface of the bed

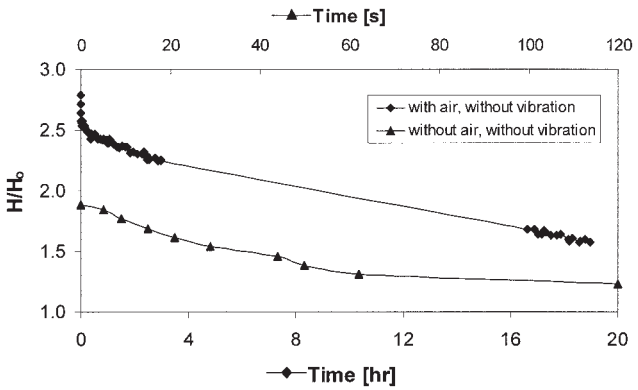

Figure 5. Bed height as a function of time.

(◆) The bed was initially subjected to vibration ($\Gamma = 2, f = 50$ Hz) and aeration at an air superficial velocity of 0.91 cm/s; at $t = 0$, the vibration was discontinued. (▲) The bed was initially subjected to vibration ($\Gamma = 2, f = 50$ Hz) and aeration at an air velocity of 0.45 cm/s; at $t = 0$, both vibration and aeration were stopped.

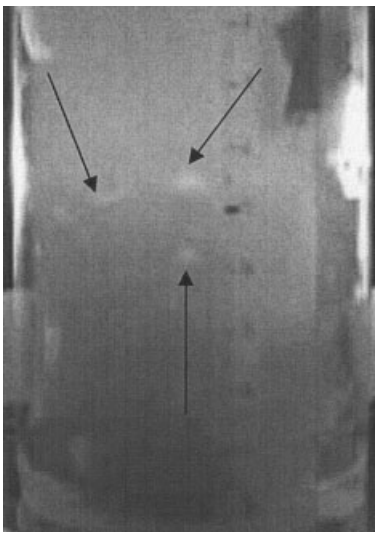

Figure 6. Bubbling fluidization in the presence of a bottom dense phase.

was very smooth, there was no apparent disturbance from bubbles, and practically no elutriation of particles was observed. At higher gas velocities (>2 cm/s), the surface became unstable and elutriation of particles out of the tube could be observed.

Figure 7a shows bed expansion rate at different Γ values at a constant frequency of 50 Hz and constant superficial air velocity of 0.28 cm/s. In each experiment, the vibrational parameters were first set at the desired conditions, and then the

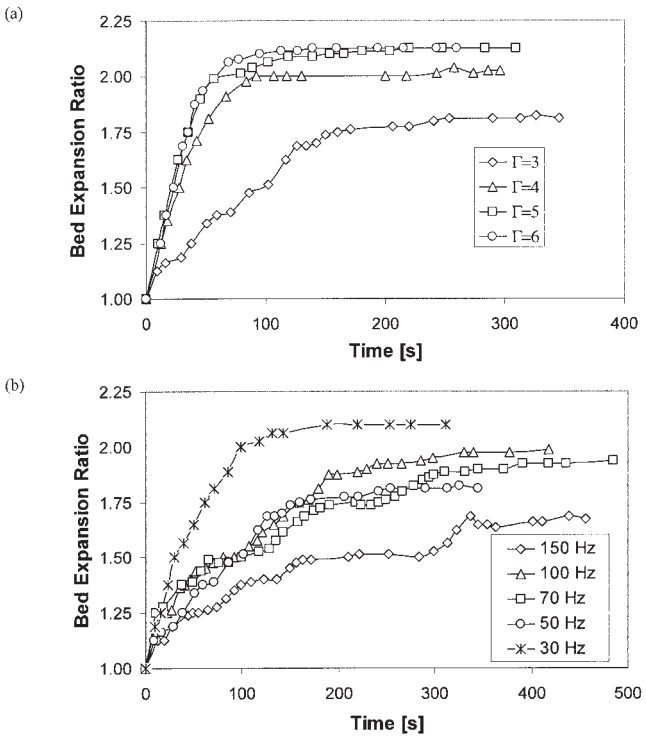

Figure 7. Plots of bed expansion ratio vs. time.

(a) For different Γ values at a fixed frequency, $f = 50$ Hz; (b) for different frequencies with $\Gamma = 3$.

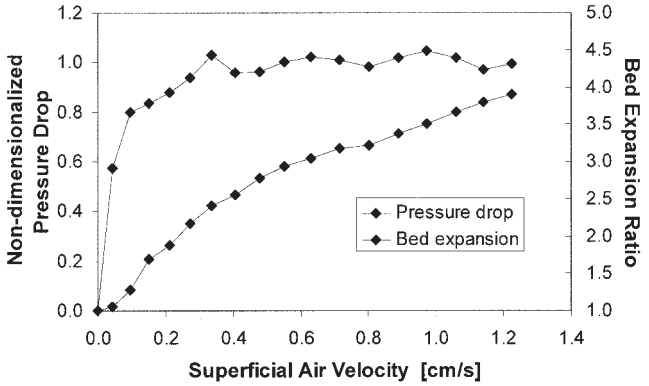

Figure 8. Pressure drop and bed expansion ratio as functions of air superficial velocity.

$\Gamma = 3$, $f = 50$ Hz.

aeration was turned on (at time $t = 0$) at the desired superficial velocity. The steady-state bed expansion increased with increasing Γ, but appeared to become independent of Γ at sufficiently large values of Γ. In this series of experiments, the vibrational intensity was varied by changing the amplitude (A), while holding the frequency of vibration constant. This bed expansion behavior may be rationalized as follows: as the vibrational intensity was increased, the size of the agglomerate decreased at first and then became roughly independent of Γ. The scaled acceleration Γ was not the only vibrational parameter affecting steady-state bed expansion. Figure 7b illustrates that the steady-state bed expansion, at a constant superficial air velocity of 0.28 cm/s, depended on the frequency of vibration, even when Γ was maintained constant; however, no systematic trend was manifest. It was found that at higher values of Γ, the effect of vibration frequency on the steady-state bed expansion decreased. It is clear from Figures 7a and b that at least two dimensionless groups involving A and ω would be needed to capture the effect of vibration on fluidization behavior.

It is also clear from Figure 7 that the rate at which the bed expanded depended on the vibrational parameters. The higher the frequency or the lower the Γ, the slower the bed expanded. The rate of bed expansion was roughly the same for $\Gamma = 4-6$, but appreciably smaller at $\Gamma = 3$ (see Figure 7a). As seen in Figure 7b, the rates of bed expansion at frequencies of 50, 70, and 100 Hz were comparable, whereas those at 30 and 150 Hz suggest an inverse dependency on the frequency.

Pressure drop

In all of the experiments performed, the measured pressure drop across the bed at high gas velocities approximately equaled the weight of the bed per unit cross-sectional area. Figure 8 shows a typical set of results obtained in a vibrated fluidized bed of silica nanopowder, where both the pressure drop across the bed and the bed expansion at increasing gas velocities are presented. The pressure drop has been scaled with the actual measured weight of the bed per unit cross-sectional area of the bed, whereas the bed height has been scaled with the height of the settled bed. It is clear from Figure 8 that the pressure drop increased initially with gas velocity and then leveled off at high gas velocities. In the plateau region, the scaled pressure drop is very close to the expected value of

unity, as given by the familiar force balance (Wilhelm and Kwauk, 1948) equation

$$\frac{\Delta P}{H_{mf}} = (1 - \varepsilon_{mf})(\rho_a - \rho_g)\, g \tag{1}$$

A lower measured pressure drop than the weight of the bed given by Eq. 1 could be attributable either to a loss of powder sticking to the wall, powder elutriation, or possibly to some nonuniformities in the gas flow resulting from the relatively porous distributor that was used in the experiments. On the other hand, wall friction (Loezos et al., 2002; Srivastava and Sundaresan, 2002) and cohesion between the bed of particles with a layer of particles adhering tightly to the distributor (Castellanos et al., 1999; Sundaresan, 2003) would result in a higher measured pressure drop than the weight of the bed.

Mutsers and Rietema (1977) were the first to suggest that additional terms may need to be included on the right-hand side of Eq. 1 to account for the higher pressure drop of cohesive powders. They developed a theory, which includes interparticle forces as well as wall friction. Liss et al. (1984) accounted for their high measured pressure drop in a fluidized bed, where the particles were cohesive because of liquid bridge formation, through a term $(6S/d_p)(1 - \varepsilon_{mf})$, which was added to Eq. 1 on the right-hand side. Here S is the cohesive stress, which is a function of temperature, composition, and particle size distribution.

Tasirin and Anuar (2001) found in their study of vibrofluidization of 15- to 34-μm particles that the pressure drop increased as the vibration intensity Γ increased. This is rather remarkable, in that it implies that the consequence of vibration was a net force pointing downward, which is not what one would expect intuitively. Erdesz and Mujumdar (1986), on the other hand, reported that the pressure drop decreased with increasing Γ. Mawatari et al. (2002) found no appreciable change in pressure drop as a function of vibration intensity Γ. Although not shown, our study revealed only a weak effect of vibrational parameters on the constant (plateau) pressure drop obtained at high gas velocities. Thus, there is no clear consensus on the effect of vibration on pressure drop across the bed.

Wank et al. (2001) studied vibrofluidization of cohesive micron-sized particles and proposed the following expression, which accounted for both interparticle forces and the effect of vibration

$$\frac{\Delta P}{H_{mf}} = (1 - \varepsilon_{mf})(\rho_a - \rho_g)g + \frac{6F_{CO}}{H_{mf}} - (1 - \varepsilon_{mf})(Af^2)\rho_a \tag{2}$$

where F_{CO} represents the interparticle forces between particles. However, in our opinion, it is hardly realistic to hope to capture the effect of cohesion and vibration through such simple models. Cohesion between particles themselves cannot increase the required pressure drop, unless the particles adhere to boundaries and a resistance to bed expansion results through this adhesion. Consequently, justification for the cohesive force term must be made through an analysis of the interaction at the boundaries. The same is true for vibration.

Figure 8 also shows that the bed-expansion behavior in our system was different from that observed with Geldart group A particles where bed expansion begins only after the minimum fluidization velocity is exceeded. As soon as a vibrofluidized bed (with $\Gamma > 1$) was aerated, it began to expand, even though the actual gas-phase pressure drop was only a fraction of the bed weight per unit cross-sectional area. As the gas flow rate was increased, the bed continued to expand and this was accompanied by a systematic increase in the gas-phase pressure drop. The bed expansion continued into the constant pressure drop regime. The overall bed expansion could be in excess of five times the original height, and even at such dramatic bed-expansion levels the quality of fluidization appeared to be smooth.

Minimum fluidization

Based on an agglomerate size of about 50 microns, the Reynolds number is less than 1. The traditional expression for calculating the minimum fluidization velocity based on the Ergun equation for $\mathrm{Re} < 20$ (Kunii and Levenspiel, 1969) is

$$u_{mf} = \frac{(\phi_s d_p)^2}{150}\frac{\rho_p - \rho_g}{\mu}\left(\frac{\varepsilon_{mf}^3}{1 - \varepsilon_{mf}}\right)g \tag{3}$$

where ϕ_s is the particle sphericity and ε_{mf} is the interparticle voidage at minimum fluidization. A number of studies (Erdesz and Mujumdar, 1986; Mawatari et al., 2002; Noda et al., 1998; Tasirin and Anuar, 2001) found that as the vibration intensity Γ increased, the minimum fluidization velocity decreased. Here, minimum fluidization velocity refers to the lowest gas velocity for which the pressure drop across the bed becomes constant. However, in our experiments (with $\Gamma > 1$), frequency and other vibrational parameters had only a slight effect on the minimum fluidization velocity, and this effect became unobservable as Γ was increased.

The minimum fluidization velocity in our study (based on the definition above) was determined to be around 0.3–0.4 cm/s (see Figure 8). However, it is noted that the bed exhibited fluidlike properties as soon as it started to expand at velocities as low as 0.1 cm/s. Such a minimum fluidization velocity cannot be obtained from Eq. 3 if we use the primary particle size, demonstrating unequivocally that we were fluidizing only agglomerates and that we must use agglomerate properties in Eq. 3 to obtain meaningful results.

Voidage

Because agglomerates were being fluidized, it is important that we carefully label various ways in which one can define voidage. We define overall voidage (ε) as the fraction of the total bed volume occupied by the fluid.

$$\varepsilon = 1 - \frac{\rho_b}{\rho_p} \tag{4}$$

Here, ρ_p and ρ_b denote the density of the primary nanoparticles and the apparent density of the bed, respectively. The volume fraction of primary particles in the bed (ϕ) is then equal to $1 - \varepsilon$. Using 0.03 and 2.2 g/cm^3 for the bulk density of a settled bed and primary nanoparticle density, respectively, one finds that $\varepsilon \sim 0.9864$. Thus, the bed of nanoparticles was already highly

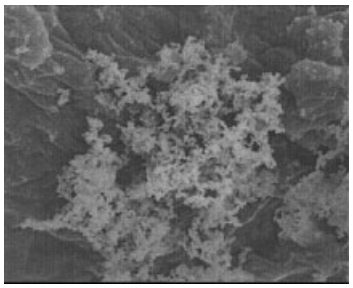

Figure 9. High-resolution SEM image of a silica agglomerate.

fluffy even before fluidization. As the bed expands, ε increases to >0.99.

The agglomerates themselves were very porous (see the high-resolution SEM image shown in Figure 9). We denote the apparent density of the agglomerates and the fraction of bed volume occupied by the agglomerates by ρ_a and ϕ_e, respectively. It then follows that $\phi\rho_p = \phi_e\rho_a$. The void space between the agglomerates, represented as a fraction of the bed volume, is expressed as $\varepsilon_e = 1 - \phi_e$. The porosity inside the agglomerates (ε_{agg}) is simply equal to $1 - \rho_a/\rho_p$.

The challenge facing us is estimation of ρ_a and ε_e from our experimental data. Chaouki et al. (1985) and Wang et al. (2002) assumed that

$$\varepsilon_e = 1 - \frac{H_0}{H_{exp}} \tag{5}$$

Equation 5 is problematic because it assigns a value of zero to ε_e for a settled bed (that is, when $H_0 = H_{exp}$). We will describe in a later section an alternate approach to estimating ρ_a and ε_e, originally presented by Valverde et al. (2001b) and Castellanos et al. (2001).

Preliminary mixing studies

A small amount of silica was dyed blue with methylene blue for mixing/tracer experiments. Figure 10 shows the progression of mixing of a small layer of blue particles placed at the top of the vibrated fluidized bed. Within a few minutes, the entire bed turned blue and appeared well mixed. Note that the aeration was applied at a level well below the minimum fluidization conditions. This showed clearly that, even in the region where the gas-phase pressure drop was considerably smaller than the bed weight per unit cross-sectional area, active mixing of the agglomerates occurred.

Preliminary SEM and EDX analyses showed that the agglomerates were well mixed, at least on the agglomerate level, indicating that vibrofluidization could be used to mix agglomerates of different species of nanoparticles. For example, we have mixed nano-silica with nano-titania and nano-molybdenum oxide. It is not known at the present time whether the agglomerates retained their integrity during fluidization or whether they broke and formed again rapidly; in the former case, one would achieve little mixing at the nanoscale. However, if mixing were indeed observed on a scale smaller than the agglomerate size, it would be indicative of fragile agglomerates, which broke and formed repeatedly in a vibrofluidized bed. Further EDX and EELS studies are currently under way to determine whether homogeneous mixing on the nanoscale can be attained.

Agglomerate size: a fractal analysis

Because the behavior of nanoagglomerate fluidization was so liquidlike with practically no bubbling, the Richardson–Zaki (R-Z) approach, usually valid for homogeneous liquid–solid sedimentation and fluidization, is used in the analysis described below. To estimate the agglomerate density and porosity in terms of its size, we use the fractal model suggested by Valverde et al. (2001b) and further explored by Castellanos et al. (2001).

Agglomerates composed of fine particles typically have fractal structures (Valverde et al., 2001b). The number of primary particles N in an agglomerate of radius r_a can be expressed as (Friedlander, 2000)

$$N = k(r_a/r_p)^{D_f} \tag{6}$$

where k is a prefactor (commonly set to unity), D_f is the fractal dimension, and r_p is the radius of the primary particle.

Assuming that the agglomerates are spherical, the mass of an agglomerate is

$$m_a = \frac{4}{3} N\pi r_p^3\rho_p = \frac{4}{3}\pi r_a^3\rho_a \tag{7}$$

Equations 6 and 7 can be combined to obtain

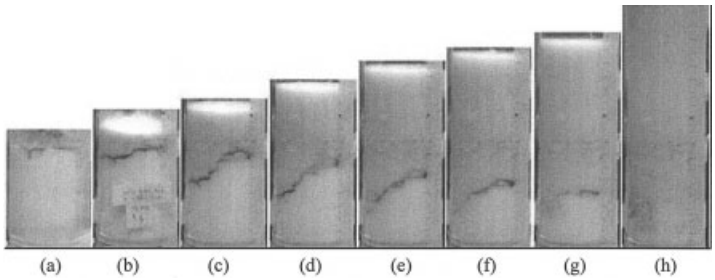

Figure 10. Progression of mixing during aerated (u = 0.45 cm/s) vibrofluidization (Γ = 4, f = 50 Hz) with time (s).

(a) 0, (b) 10, (c) 15, (d) 22, (e) 28, (f) 35, (g) 60, and (h) 120. Aeration of a vibrated fluidized bed was started at $t = 0$, and the figure panels show simultaneous bed expansion and mixing.

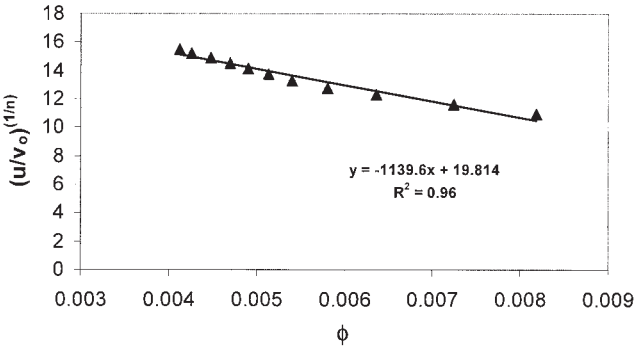

Figure 11. Plot of Eq. 12 for $n = 5$ to obtain agglomerate size, density, and interparticle voidage.

R^2 is the square of the correlation from a simple linear regression model that measures the amount of variability in the observed data.

$$\frac{\rho_a}{\rho_p} = N^{1-(3/D_f)} \tag{8}$$

It then follows that

$$\phi_e = \phi N^{(3/D_f)-1} \tag{9}$$

The Stokes settling velocities of a primary particle (V_0) and that of an agglomerate (v_a) are $C(2\rho_p r_p^2 g/9\mu)$ and $2\rho_a r_a^2 g/9\mu$, respectively, where C is the Cunningham correction factor which applies for particles less than 1 μm in diameter (Seinfeld, 1986). These velocities can be combined with Eq. 6 to obtain

$$v_a = \frac{V_0}{C}\frac{\rho_a}{\rho_p}\left(\frac{r_a}{r_p}\right)^2 = v_0 N^{1-(1/D_f)} \tag{10}$$

where $v_0 = 2\rho_p r_p^2 g/9\mu$. Using Eqs. 9 and 10, the R-Z equation, that is

$$\frac{u}{v_a} = \varepsilon_e^n$$

where n is the R-Z exponent, can be written as

$$u = v_0 N^{1-(1/D_f)}(1 - \phi N^{(3/D_f)-1})^n \tag{11}$$

For each value of u, ϕ was determined from the measured bed height. Equation 11 indicates that a plot of $(u/v_0)^{1/n}$ vs. ϕ for a reasonable value of n would yield a linear relationship with a y-intercept b, equal to $N^{[1-(1/D_f)](1/n)}$ and a slope m, equal to $-bN^{(3/D_f)-1}$. The radius of the agglomerate can then be calculated from

$$r_a = r_p\sqrt{-mb^{n-1}} \tag{12}$$

One such plot, for $n = 5$ (the R-Z exponent is a function of Reynolds number, but is about 4.8 in the viscous flow regime) based on the experimental data given in Figure 8 is shown in Figure 11. The plot appears to be reasonably linear, lending support to such an analysis.

Table 1. Fractal Dimension (D_f), Number of Particles in an Agglomerate (N), and Agglomerate Diameter for Various Values of the Richardson–Zaki Exponent

n	D_f	N	Calculated Diameter (microns)
4.0	2.5596	3.835E+10	164
4.5	2.5666	3.955E+10	161
5.0	2.5731	4.047E+10	159
5.5	2.5791	4.117E+10	157
6.0	2.5848	4.169E+10	154

Surprisingly, the fractal dimension, number of primary particles, and diameter of the agglomerates were found to be insensitive to the value of the R-Z exponent with n values ranging from 4 to 6 (see Table 1).

The estimated value of 2.57 for the fractal dimension is close to that for diffusion-limited aggregation (that is, 2.5) (Friedlander, 2000). Given that such an aggregation mechanism is reasonable for the extremely fine primary particles used in our study, the fractal dimension estimated from the bed height data and the above analysis is very encouraging. However, the estimated agglomerate diameter (~160 microns) is much larger than the experimentally measured value, which SEM photographs, showed to be about 30 microns, but in good agreement with the bright agglomerates seen in Figure 4, obtained by photographing the surface of the bed using a high-speed digital camera with an extremely short exposure time. We suspect that considerable breakage of the fragile porous agglomerates took place when we aspirated the particles out of the bed and/or prepared the samples for SEM analysis. This might explain why our experimental SEM agglomerate sizes were much smaller than those estimated from the fractal analysis; however, this issue remains unresolved at this point.

Using an agglomerate diameter of 160 microns and the experimental pressure drop data, we estimated ε_e at various gas velocities through the Blake–Kozeny equation (Ergun equation at low Reynolds numbers), as follows:

$$\frac{\Delta P}{H} g_c = 150\frac{(1-\varepsilon_e)^2}{\varepsilon_e^3}\frac{\mu u_0}{(\phi_s d)^2} \tag{13}$$

Table 2 compares the values of ε_e determined through the three methods mentioned above: (1) the modified Richardson–Zaki analysis, which used only the bed-expansion data; (2) the

Table 2. Summary of Interagglomerate Voidages Calculated from the Modified Richardson–Zaki Method, Blake–Kozeny Equation, and Eq. 6

u (cm/s)	ε_e (Modified Richardson–Zaki)	ε_e (Blake–Kozeny Equation)	$\varepsilon_e = 1 - H_0/H_{exp}$
0.149	0.529	0.526	0.400
0.207	0.584	0.566	0.469
0.268	0.634	0.602	0.534
0.331	0.666	0.632	0.574
0.399	0.689	0.657	0.603
0.469	0.704	0.677	0.623
0.542	0.718	0.700	0.641
0.619	0.729	0.709	0.655
0.700	0.742	0.724	0.671
0.785	0.755	0.738	0.688
0.870	0.763	0.741	0.697

pressure drop data, which assumed an agglomerate size estimated from the Richardson–Zaki analysis; and (3) the simple approach used by Chaouki et al. (1985) and Wang et al. (2002) (that is, Eq. 5). Table 2 corresponds to the data presented earlier in Figure 8. It is clear from Table 2 that the values of ε_e determined by the first two methods are close to each other (except at the lower end of voidage), which lends further support to the fractal approach. We could have demanded that both the pressure drop and bed-expansion data be satisfied accurately by the model and allowed the agglomerate size to vary (slightly) with gas velocity. Such an exercise (details of which are not presented here) revealed that the agglomerate size decreases slightly as the gas velocity is increased, which is physically reasonable.

The third method, using Eq. 5, gave quite reasonable values of ε_e for values of $H/H_0 > 2$ (Table 2), but gave very small (and unphysical) values of ε_e at lower gas velocities, which will be shown in subsequent tables.

We performed a fractal analysis (coupled with the R-Z equation) for the bed-expansion data of Wang et al. (2002). This research group used Aerosil R972, which is very similar to Aerosil R974, used in our experiments. For R-Z exponents of 3.5, 4.0, 4.5, and 5.0, the D_f values were found to be 2.5304, 2.5386, 2.5461, and 2.5529 and the radii of the agglomerates calculated were 140, 135, 130, and 126 microns, respectively. The values of ε_e estimated from the data by Wang et al. (2002), assuming a value of 5 for the R-Z exponent, are summarized in Table 3. Also listed are the values of ε_e obtained by Wang et al. (2002) by using Eq. 5.

Wang et al. (2002) also performed experiments with other nanoparticles. Aerosil 300, for example, whose apparent density and primary particle size are 37 kg/m^3 and 7 nm, respectively, did not exhibit high (>2) bed-expansion ratios. They applied Eq. 5 and obtained ε_e values summarized in Table 4.

When we performed a fractal analysis of the same data, assuming that $n = 5$, more reasonable estimates for ε_e were obtained (see Table 4). This example shows that Eq. 5 cannot be used to estimate ε_e when the bed expansion is low but is a fair approximation for bed expansions > 2.

It is important to note that the data from Wang et al. (2002) are from fluidization experiments at relatively high flow rates of the fluidizing gas without the aid of vibration. Their results show that a much higher superficial velocity (which could result in significant elutriation) is needed to achieve fluidization than that in the vibrofluidized bed, which we used in our experiments.

Table 3. Interagglomerate Voidages Obtained from Modified Richardson–Zaki Method and Eq. 6 for Aerosil R972*

u (cm/s)	ε_e (Modified Richardson–Zaki)	$\varepsilon_e = 1 - H_0/H_{exp}$
1.45	0.735	0.643
1.7	0.772	0.692
2.15	0.797	0.726
2.4	0.819	0.756
2.7	0.835	0.778

*Wang et al. (2002).

Table 4. Interagglomerate Voidages Obtained from Modified Richardson–Zaki Method and Eq. 6 for Aerosil 300*

u (cm/s)	ε_e (Modified Richardson–Zaki)	$\varepsilon_e = 1 - H_0/H_{exp}$
3.00	0.783	0.329
3.49	0.801	0.383
3.90	0.816	0.429
4.70	0.849	0.535
5.50	0.885	0.643
6.25	0.902	0.697

*Wang et al. (2002).

Concluding Remarks

We have demonstrated that nanosized silica could be easily and smoothly fluidized in the form of stable, very porous agglomerates with negligible elutriation with the aid of vibration and aeration. Because the bed remained fluidized for a considerable amount of time with only air flow after vibration was turned off, vibration appeared to be necessary only initially to disrupt interparticle networks, after which aeration was sufficient to sustain the bed in a fluidized and expanded state for an extended period of time. Our mixing studies suggest that the application of vibrofluidization of nanoparticles to mix different nanoparticles together to form nanocomposites is a promising approach. A modified Richardson–Zaki approach combined with an assumption of fractal agglomerates was successfully applied to analyze the bed-expansion data reported here, from which we estimated the agglomerate size, other agglomerate properties, and the interagglomerate voidage. The pressure drop data were found to be consistent with agglomerate size determined in this manner.

Future work should examine vibrofluidization of different powders (to probe how the size and nature of the primary particles affect the agglomerate size, etc.), the effect of different fluidizing gases on the behavior of vibrofluidization, and the effect of different types of distributors and different tube diameters to see whether these have any effect on the plateau pressure drop observed in our studies. It is also important to determine the scale at which mixing of two different nanostructured materials occurs and to improve the method of measuring the dynamic agglomerate size in situ.

Acknowledgments

We gratefully acknowledge the National Science Foundation for financial support through Grant 0210400, NIRT–Collaborative Research: Experimental and Computational Investigations of Fluid Interactions/Transport in Nanodomains and Around Nanoparticles. We also express our appreciation to the New Jersey Commission of Science and Technology for their financial support, especially during the initial stages of this research. Special thanks are also due to Dr. Herbert Riemenschneider of Degussa for supplying us with different nanoparticles and to Prof. John A. Dodds and Dr. Alain de Ryck for their hospitality and for allowing us to use the laboratory facilities at L'Ecole des Mines d'Albi Carmaux, where the first two authors spent 3 months during the Spring of 2002. S.S. gratefully acknowledges support of his efforts by the Merck Foundation.

Notation

A = amplitude of vibration, m
C = Cunningham correction factor
d_p = diameter of primary particle, m
d_a = diameter of agglomerate, m
D_f = fractal dimension of an agglomerate

f = frequency, Hz
g = acceleration of gravity, m/s^2
H = Hamaker constant
H_{exp} = height of expanded bed at a certain air velocity, m
H_{mf} = height of bed at minimum fluidization, m
H_0 = initial (settled) height of bed before fluidization experiment, m
m_a = mass of an agglomerate, kg
n = Richardson–Zaki exponent
N = number of particles in an agglomerate
ΔP = pressure drop, Pa
r_a = radius of the agglomerate, m
r_p = radius of the primary particle, m
u = superficial velocity, m/s
u_{mf} = minimum fluidization velocity, m/s
v_a = Stokes' settling velocity of an agglomerate, m/s
V_0 = Stokes' settling velocity of a primary particle, including the Cunningham correction factor, m/s
$v_0 = V_0/C$, m/s

Greek letters

α = cross-sectional area, m^2
ε = total bed voidage
ε_e = interagglomerate voidage
ε_{mf} = total voidage at minimum fluidization
Γ = vibration intensity
ϕ_e = volume fraction of agglomerates in the bed
ϕ = volume fraction of primary particles in the bed
ϕ_s = sphericity of particle
ρ_a = density of agglomerate, kg/m^3
ρ_p = density of primary particle, kg/m^3
ρ_g = density of fluidizing gas, kg/m^3
ω = angular velocity = $2\pi f$ (radians/s)

Literature Cited

Castellanos, A., J. M. Valverde, and M. A. S. Quintanilla, "Aggregation and Sedimentation in Gas-Fluidized Beds of Cohesive Powders," *Phys. Rev. E.*, **64**, 041304, 1 (2001).

Chaouki, J., C. Chavarie, and D. Klvana, "Effect of Interparticle Forces on the Hydrodynamic Behavior of Fluidized Aerogels," *Powder Technol.*, **43**, 117 (1985).

Chirone, R., L. Massimilla, and S. Russo, "Bubble-Free Fluidization of a Cohesive Powder in an Acoustic Field," *Chem. Eng. Sci.*, **48**, 41(1993).

Dutta, A., and L. V. Dullea, "Effects of External Vibration and the Addition of Fibers on the Fluidization of a Fine Powder," *AIChE Symp. Ser.*, **87**, 38 (1991).

Erdesz, K., and A. S. Mujumdar, "Hydrodynamic Aspects of Conventional and Vibrofluidized Beds—A Comparative Evaluation," *Powder Technol.*, **46**, 167 (1986).

Friedlander, S. K., *Smoke, Dust, and Haze: Fundamentals of Aerosol Dynamics*, Oxford University Press, New York (2000).

Geldart, D., "Types of Gas Fluidization," *Powder Technol.*, **7**, 285 (1973).

Herrera, C. A., E. K. Levy, and J. Ochs, "Characteristics of Acoustic Standing Waves in Fluidized Beds," *AIChE J.*, **48**, 503 (2002).

Iwadate, Y., and M. Horio, "Prediction of Agglomerate Sizes in Bubbling Fluidized Beds of Group C Powders," *Powder Technol.*, **100**, 223 (1998).

Jaraiz, E., S. Kimura, and O. Levenspiel, "Vibrating Beds of Fine Particles: Estimation of Interparticle Forces from Expansion and Pressure Drop Experiments," *Powder Technol.*, **72**, 23 (1992).

Kunii, D., and O. Levenspiel, *Fluidization Engineering*, Wiley, New York (1969).

Li, H., R. Legros, C. M. H. Brereton, J. R. Grace, and J. Chaouki, "Hydrodynamic Behavior of Aerogel Powders in High-Velocity Fluidized Beds," *Powder Technol.*, **60**, 121 (1990).

Liss, B., T. R. Blake, A. M. Squires, and R. Bryson, "Incipient Defluidization of Sinterable Solids," Proc. 4th Int. Conf. Fluid., 249 (1984).

Loezos, P. N., P. Costamagna, and S. Sundaresan, "The Role of Contact Stresses and Wall Friction on Fluidization," *Chem. Eng. Sci.*, **57**, 5123 (2002).

Malhotra, K., and A. S. Mujumdar, "Immersed Surface Heat Transfer in a Vibrated Fluidized Bed," *Ind. Eng. Chem. Res.*, **26**, 1983 (1987).

Marring, E., A. C. Hoffmann, and L. P. B. M. Janssen, "The Effect of Vibration on the Fluidization Behaviour of Some Cohesive Powders," *Powder Technol.*, **79**, 1 (1994).

Marring, E., A. C. Hoffmann, and L. P. B. M. Janssen, "A Study of Discharge of Cohesive Powders under Simultaneous Aeration and Vibration," *Particulate Sci. Technol.*, **13**, 7 (1995).

Mawatari, Y., T. Koide, Y. Tatemoto, S. Uchida, and K. Noda, "Effect of Particle Diameter on Fluidization under Vibration," *Powder Technol.*, **123**, 69 (2002).

Mori, S., A. Yamamoto, S. Iwata, T. Haruta, and I. Yamada, "Vibrofluidization of Group-C Particles and Its Industrial Applications," *AIChE Symp. Ser.*, **86**, 88 (1990).

Morooka, S., K. Kusakabe, A. Kobata, and Y. Kato, "Fluidization State of Ultrafine Powders," *J. Chem. Eng. Jpn.*, **21**, 41 (1988).

Mutsers, S. M. P.; and K. Rietema, "The Effect of Interparticle Forces on the Expansion of a Homogeneous Gas-Fluidized Bed," *Powder Technol.*, **18**, 239 (1977).

Noda, K., Y. Mawatari, and S. Uchida, "Flow Patterns of Fine Particles in a Vibrated Fluidized Bed under Atmospheric or Reduced Pressure," *Powder Technol.*, **99**, 11 (1998).

Pacek, A. W., and A. W. Nienow, "Fluidization of Fine and Very Dense Hardmetal Powders," *Powder Technol.*, **60**, 145 (1990).

Seinfeld, J. H., *Atmospheric Chemistry and Physics of Air Pollution*, Wiley, New York. p. 317 (1986).

Srivastava, A., and S. Sundaresan, "Role of Wall Friction in Fluidization and Standpipe Flow," *Powder Technol.*, **124**, 45 (2002).

Sundaresan, S., "Instabilities in Fluidized Beds," *Ann. Rev. Fluid Mech.*, **35**, 63 (2003).

Tasirin, S. M., and N. Anuar, "Fluidization Behavior of Vibrated and Aerated Beds of Starch Powders," *J. Chem. Eng. Jpn.*, **34**, 1251 (2001).

Valverde, J. M., A. Castellanos, and M. A. S. Quintanilla, "Effect of Vibration on the Stability of a Gas-Fluidized Bed of Fine Powder," *Phys. Rev. E*, **64**, 021302 (2001a).

Valverde, J. M., M. A. S. Quintanilla, A. Castellanos, and P. Mills, "The Settling of Fine Cohesive Powders," *Europhysics Lett.*, **54**, 3, 329 (2001b).

Venkatesh, R. Deiva, M. Grmela, and J. Chaouki, "Simulations of Vibrated Fine Powders," *Powder Technol.*, **100**, 211 (1998).

Wang, Y., G. Gu, F. Wei, and J. Wu, "Fluidization and Agglomerate Structure of SiO_2 Nanoparticles," *Powder Technol.*, **124**, 152 (2002).

Wang, Z., M. Kwauk, and H. Li, "Fluidization of Fine Particles," *Chem. Eng. Sci.*, **53**, 377 (1998).

Wank, J. R.; S. M. George, and A. W. Weimer, "Vibro-fluidization of Fine Boron Nitride Powder at Low Pressure," *Powder Technol.*, **121**, 195 (2001).

Wilhelm, R. M., and M. Kwauk, "Fluidization of Solid Particles," *Chem. Eng. Prog.*, **48**, 201 (1948).

Youzhi, L., Z. Jiyu, and Z. Bijiang, "Separation of a Binary Particle Mixture in a Vibrating Fluidized Bed of Dense Medium," *Powder Technol.*, **100**, 41 (1998).

Zhou, T., and H. Li, "Estimation of Agglomerate Size for Cohesive Particles during Fluidization," *Powder Technol.*, **101**, 57 (1999).

Manuscript received May 5, 2003, revision received Oct. 29, 2003, and final revision received Jan. 30, 2004.